19th Brazilian Congress of Thermal Sciences and Engineering
November 06th-10th, 2022, Bento Gonçalves - RS - Brazil

ENC-2022-0219
ASSESSMENT OF THE STEAM REFORMING OF ETHANOL FOR HYDROGEN PRODUCTION IN A LUMPED-PARTICLE PACKED BED REFORMER HEATED BY MOLTEN SALT

Marcos Alberto Feitoza e Silva
Daniel Ribeiro Dessaune
Renato da Silva Pereira
Jornandes Dias da Silva
Polytechnic School - UPE, Laboratory of Environmental and Energetic Technology; Rua Benfica - 455, Madalena, Recife – PE, Brazil, Cep: 50750-470
albertomafs87@gmail.com
drd1@poli.br
rsp1@poli.br
jornandesdias@poli.br

Abstract. *The steam reforming of ethanol (SRE) is currently considered a promising process for so-called synthesis gas (H_2 and CO). The synthesis gas (syngas) can be obtained from various fuels among which natural gas is of special importance. The SRE can be processed on the porous materials bed as solid open-cell foams due to high porosity and great surface area. Solid open-cell foams are macroporous reticulated 3D structures constituted by interconnected cavities and made of metals (aluminum, steel), ceramics (alumina, silicon carbide etc.), or carbon materials. The Lumped-Particle Packed Bed (LPPB) Reformers have been substantially studied in the past years as a promising reformer to study the thermochemical conversion of ethanol. A variety of researches have been approached in the experimental field and theoretical. This work has as main objective a theoretical modelling to describe the process variables of the SRE on the LPPB reformer. These process variables describe the specific aims as from each equation of a physical-mathematical model characterizing the performance from reformer. When the C_2H_5OH/H_2O ratio decreases on the SRE method in LPPB reformer, the reaction temperature is notably increased. An increase of the $u_{g,avg}$ indicates a decrease on the reaction temperature profiles in LPPB reformer and, thus, a reduction in the heat release by the SRE method. An increase of the operating temperature has a significant role of the thermochemical conversion of C_2H_5OH because of the higher consumption of reactants in reforming method from the SRE.*

Keywords: *Ethanol, Steam reforming, Modelling, Packed bed, Simulation*

1. INTRODUCTION

Renewable energy sources have been considered to be as one of the most efficiency solutions to reach the targets of the production of green hydrogen (H_2). Because of the limitations of the production of H_2 from organic compounds and water, various sources such as coal, natural gas, liquefied petroleum gas, propane, methane, gasoline, biomass-derived liquid fuels (e.g. methanol, ethanol (C_2H_5OH), biodiesel) have been explored for H_2 extraction. Among these sources, C_2H_5OH can be an excellent candidate for the production of H_2 due to its renewability, facility of access and transport, biodegradability, low toxicity, neither need for catalytic toxins, and ease of decomposition. The technology of the reforming process in a thermochemical reformer contributes to the key innovative element of sustainable development (Dias and Silva, 2020; Lima et al., 2020). Steam Reforming of Ethanol (SRE) can be implemented in a Lumped-Particle Packed Bed (LPPB) reformer to produce syngas. Syngas is a precious inflammable gas mixture of H_2 and carbon monoxide (CO) and smaller quantities of methane, carbon dioxide and hydrocarbons (Cruz and Silva, 2017). The overall reaction of C_2H_5OH reacts with a steam stream of water (H_2O) at moderate temperature to form syngas mixture (H_2, CO). Its benefit is that is does not request oxygen and operate at relatively lower operating temperature.

The global energy system depends mainly on fossil fuels that unload an enormous amount of greenhouse gases (GHG) and other environmental pollutants. To minimize the emissions of pollutant gases, researchers have been concentrating on developing renewable energy sources for energy generation (Aron et al., 2020). The thermochemical reforming technology can be used to produce renewable energies (as hydrogen (H_2) production) from chemical reaction

processes. The utilization of H_2 is increasing in many countries due to potential decarbonization and sustainable energy transition designs (Chein et al., 2017). H_2 is shown to be a versatile transition alternative in different applications, with an increasing trend towards cleans alternatives with better performance improving the existing processes. The production process of H_2 followed worldwide includes the use of fossil fuels as raw materials or as energy (Silva and Abreu, 2016). The disadvantages of the reforming process from fossil are the contribution of emissions of GHG into the environment.

The global process of steam reforming of C_2H_5OH is highly endothermic. The heat required for this reaction can be supplied by a thermal furnace turned on reformer. Mathematical modelling is built at non-isothermal conditions due to endothermic process of chemical reaction (Silva and Abreu, 2016, Villafán-Vidales et al., 2017). The mathematical model developed for this work involves non-steady-state, non-isothermal, and one-dimensional conditions. From the point of theoretical view, the one-dimensional model includes the gas-phase temperature, solid-phase temperature, the reactants in the reforming process of C_2H_5OH are C_2H_5OH, C_2H_5OH gas, and water vapor (H_2O), and its products are carbon dioxide (CO_2), and H_2. The governing equations of the mathematical modelling consist of an energy balance of the gas phase, energy balance of the solid phase, mass balance of C_2H_5OH, mass balance of H_2O, mass balance of CO_2, and mass balance of H_2. In addition, energy balances of molten salt in heating tube are considered in mathematical modelling.

This work reports the mathematical modelling of the SRE process in a LPPB reformer. The main aim of this study is to investigate the heat and mass transfer phenomena coupled with thermochemical reaction kinetics from SRE. The performance from LPPB reformer using the reforming process is numerically investigated in terms of the temperature profiles of the endothermic reaction. On the other hand, it was also studied the reactant and product distribution as well as the conversion of C_2H_5OH and production of H_2 in LPPB reformer.

2. DESCRIPTION OF THE PHYSICAL PROBLEM

Thermal energy storage in molten salt plays an important role in some industrial applications such as solar thermal storage. A heating tube (with molten salt) turned on to LPPB reformer provides efficient thermal energy due to their high heat transfer effectiveness (Sun et al., 2022; He et al., 2022). The thermal energy stored inside thermal insulation (molten salt) is transferred towards reformer's packed bed where the reaction of C_2H_5OH occurs. The schematic setup from Figure 1 shows the general structure of the packed bed thermal storage system. In this setup, an energy source is turned on to heating tube to keep dynamic thermal storage in the LPPB reformer.

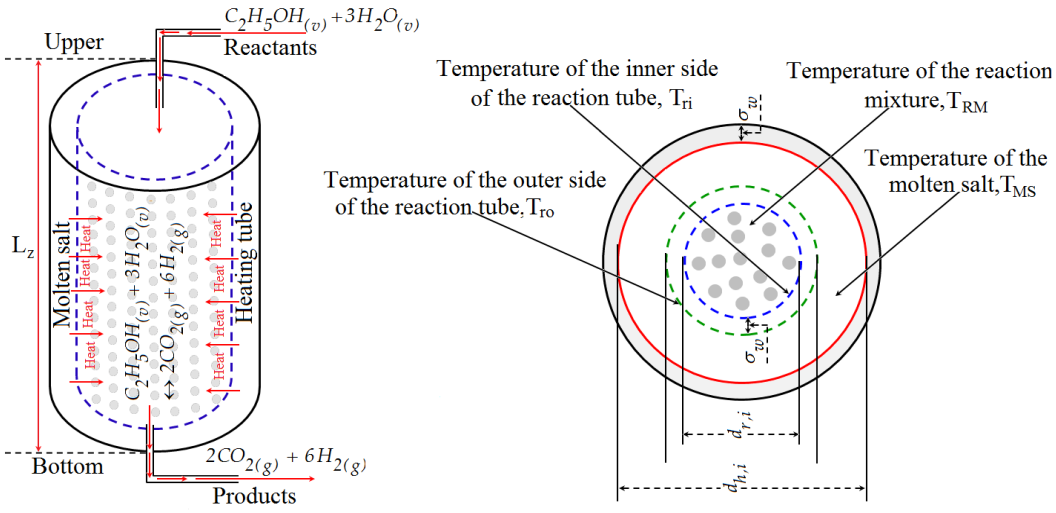

Figure 1. Schematic setup of packed bed thermal storage system.

3. DIRECT PROBLEM

3.1 Methodology

The schematic setup from Figure 1 involves a heating tube (with molten salt) as thermal insulation and LPPB reformer, respectively. The methodology reported in this work consists of the following steps: (i) kinetic model of the SRE, (ii) energy balances of the molten salt inside heating tube, (iii) energy balance of the gas phase, energy balance of the solid phase, mass balance of the reactants, and mass balance of products in LPPB reformer.

3.2 Kinetic mechanism

The reforming reaction of C_2H_5OH is highly endothermic and it can be used to produce H_2 and syngas (H_2 e CO) at moderate temperature. As the reforming process of C_2H_5OH is strongly endothermic, the thermodynamic equilibrium of this reaction dependent on the operating temperature and its global reaction is given as follows.

$$C_2H_5OH_{(v)} + 3H_2O \rightleftarrows 2\,CO_{2(g)} + 6H_{2(g)};\ \Delta H^0_{298\,K} = +157.09\,kJ/mol \tag{1}$$

3.3 Kinetic model

The overall rate equation of the reaction was developed based on Langmuir-Hinshelwood kinetic model and can be met in Sahoo et al., (2007) as follows.

$$R_{SRE} = \frac{k_{SRE}\,K_{C_2H_5O_{(1)}}\left(\frac{P_{C_2H_5OH}}{P_{H_2}^{1/2}}\right)\left[1-\left(\frac{P_{H_2}^4\,P_{CO_2}^2}{K_r\,P_{H_2O}^2\,P_{C_2H_5OH}}\right)\right]}{\beta_{EN.}}\left(C_{S1}^T\right)^2 \tag{2}$$

Where β_{EN} is given as follows.

$$\beta_{EN} = 1 + K_{CO_2(1)}P_{CO_2} + K_{CO(1)}P_{CO} + K_{CH_4(1)}P_{CH_4} + K_{HCOO(1)}P_{H_2}^{1/2}P_{CO_2} + K_{H_{2(1)}}P_{H_2}^{1/2} + \frac{K_{C_2H_4O(1)}P_{H_2}^5\,P_{CO_2}^2}{P_{H_2}^3} + \frac{K_{C_2H_5O(1)}P_{C_2H_5OH}}{P_{H_2}^{1/2}} + \frac{K_{HO(1)}P_{H_2O}}{P_{H_2}^{1/2}} \tag{3}$$

$$K_r = \frac{K_{C_2H_5O(1)}\left(\frac{k_{SRE}}{K_{-SRE}}\right)}{K_{C_2H_4O(1)}\,K_{H_{2(1)}}} \tag{4}$$

3.4 Heat and mass transfer

The gas-solid reaction of C_2H_5OH at the surface of solid particles of the packed bed involves the heat and mass transfer process along the LPPB reformer. A comprehensive mathematical model is developed based on the heat and mass physical phenomena to analyze and predict the performance of the LPPB reformer in the use of the SRE process as an important process for hydrogen production. A 1D non-isothermal model is built based on energy and mass balance equations through the heating tube (with molten salt) and lumped-particles packed bed. o simplify the model development, several assumptions are considered as follows: (a) dynamic-estate condition, (b) negligible pressure drop, (c) axial diffusion along the LPPB reformer, (d) negligible convective radial dispersion, (e) negligible heat and mass transfer diffusion inside the catalyst pellets.

3.5 Governing equations of the heat transfer in the heating tube

An energy balance equation is developed based on temperature of the gas phase inside the heating tube. As the temperature indicates the thermal energy storage in other substance, an energy balance equation is also built based on temperature of the molten salt particles in the heating tube. The governing energy balances for the gaseous phase and molten salt particles are reported as follows.

- Energy equation for the water steam;

$$\varepsilon_t\,\rho_v\,C_{p,v}\left(\frac{\partial T_{t,v}}{\partial t} + u_v\frac{\partial T_{t,v}}{\partial z}\right) = \varepsilon_t\,\lambda_v\frac{\partial^2 T_{t,v}}{\partial z^2} + h_v\left(T_{salt} - T_{t,v}\right) + \frac{2h_w}{R_{in.}}\left(T_{t,v} - T_{rm}\right) \tag{5}$$

- Initial and boundary conditions for Equation (5) are defined as;

$$T_{t,v}\Big|_{t=0} = T_{t,v,0} \tag{6}$$

$$\lambda_s \frac{\partial T_{t,v}}{\partial z}\bigg|_{z=0^+} = \rho_s C_{p,v} \frac{4Q_{t,v}}{\pi d_{t,in.}^2}\left(T_{t,v}\Big|_{z=0^+} - T_{v,in.}\right) \tag{7}$$

$$\frac{\partial T_{t,v}}{\partial z}\bigg|_{z=L} = 0 \tag{8}$$

- Energy equation for the molten salt;

$$\left(1-\varepsilon_t\right)\rho_{salt} C_{p,salt} \frac{\partial T_{salt}}{\partial t} = \left(1-\varepsilon_t\right)\lambda_{salt} \frac{\partial^2 T_{salt}}{\partial z^2} + h_v\left(T_{t,v} - T_{salt}\right) \tag{9}$$

- Initial and boundary conditions for Equation (9) are defined as;

$$T_{salt}\Big|_{t=0} = T_{salt,0} \tag{10}$$

$$T_{salt}\Big|_{z=0^+} = T_{salt,in.} \tag{11}$$

$$\frac{\partial T_{salt}}{\partial z}\bigg|_{z=L} = 0 \tag{12}$$

3.6 Governing equations of the heat transfer in the LPPB reformer

An energy balance equation is developed based on temperature of the gas phase inside the LPPB reformer. The governing energy balance based on gaseous phase is shown as follows.

- Energy balance equation for the gaseous phase in the LPPB reformer;

$$\varepsilon_b \rho_{g,mix.} C_{p,mix.}\left(\frac{\partial T_{rm}}{\partial t} + u_g \frac{\partial T_{rm}}{\partial z}\right) = \varepsilon_b \lambda_{ax,eff} \frac{\partial^2 T_{rm}}{\partial z^2} + h_{gs} \frac{6}{d_p} \frac{\left(1-\varepsilon_b\right)}{\varepsilon_b}\left(T_{rm} - T_s\right) + \frac{2h_w}{R_{in.}}\left(T_{rm} - T_{t,v}\right) \tag{13}$$

- Initial and boundary conditions for Equation (13) are defined as;

$$T_g\Big|_{t=0} = T_{g,0} \tag{14}$$

$$\frac{\partial T_g}{\partial z}\bigg|_{z=0^+} = \frac{u_g \rho_{mix.} C_{p,mix.}}{\lambda_{g,mix.}}\left(T_g\Big|_{z=0^+} - T_{g,\infty}^{Upper}\right) \tag{15}$$

$$\frac{\partial T_g}{\partial z}\bigg|_{z=L_z} = \frac{h_{gs,eff}}{\lambda_{g,mix.}}\left(T_{g,\infty}^{Bottem} - T_g\Big|_{z=L_z}\right) \tag{16}$$

On the other hand, an energy balance equation is also developed to report the temperature in the solid phase along the LPPB reformer as follows.

- Energy balance equation for the solid phase in the LPPB reformer;

$$\rho_s C_{p,s} \frac{\partial T_s}{\partial t} = \lambda_{s,eff} \frac{\partial^2 T_s}{\partial z^2} + h_{sg} \frac{6}{d_p} \frac{\left(1-\varepsilon_b\right)}{\varepsilon_b} \left(T_s - T_{rm}\right) + \rho_s \frac{\left(1-\varepsilon_p\right)}{\varepsilon_p} \eta_{SRE} R_{SRE} \left(2\Delta H^0_{CO_2,(g)} + 6\Delta H^0_{H_2,(g)} - \Delta H^0_{C_2H_5OH,(v)} - 3\Delta H^0_{H_2O,(v)} \right) \tag{17}$$

- Initial and boundary conditions for Equation (17) are defined as;

$$T_s\Big|_{t=0} = T_{s,0} \tag{18}$$

$$T_s\Big|_{z=0^+} = T_{s,in.} \tag{19}$$

$$\left.\frac{\partial T_s}{\partial z}\right|_{z=L_z} = \frac{h_{sg,eff}}{\lambda_{s,eff}} \left(T^{Bottem}_{s,\infty} - T_s\Big|_{z=L_z} \right) \tag{20}$$

3.7 Mass transfer in the gas phase inside the LPPB reformer

A mass balance equation in the gas phase will accounts chemical components (i = C_2H_5OH, H_2O, CO_2 and H_2) of Equation (1) along the axial direction of the LPPB reformer. However, the concentration distributions of each chemical component in the gas phase can be determined from following equation.

- Mass balances of each chemical component in the gaseous phase are given as;

$$\frac{\partial C_{g,i}}{\partial t} = D_{ax,g,i} \frac{\partial^2 C_{g,i}}{\partial z^2} - u_g \frac{\partial C_{g,i}}{\partial z} + k_{gs,i} \frac{3}{R_p} \frac{\left(1-\varepsilon_b\right)}{\varepsilon_b} \left(C_{g,i} - C_{s,i}\Big|_{r=R_p} \right) \tag{21}$$

- Initial and boundary conditions for Equation (21) are defined as;

$$C_{g,i}\Big|_{t=0} = C_{g,i,0} \tag{22}$$

$$\varepsilon_b D_{ax,g,i} \left.\frac{\partial C_{g,i}}{\partial z}\right|_{z=0^+} = u_g \left(C_{g,i}\Big|_{z=0^+} - C^{Upper}_{g,i,\infty} \right) \tag{23}$$

$$\varepsilon_b D_{ax,g,i} \left.\frac{\partial C_{g,i}}{\partial z}\right|_{z=L_z} = k_{gs,i,eff} \left(C_{g,i}\Big|_{z=L_z} - C^{Bottem}_{g,i,\infty} \right) \tag{24}$$

3.8 Mass transfer at the surface of the solid phase inside the LPPB reformer

To simplify the problem, it is assumed that the reforming reaction of C_2H_5OH occurs at the surface of solid particles from lumped-particle packed bed. Therefore, the governing equation of chemical components at the surface of solid particles is given as follows.

$$k_{gs,i} \frac{3}{R_p} \frac{\left(1-\varepsilon_b\right)}{\varepsilon_b} \left(C_{s,i}\Big|_{r=R_p} - C_{g,i} \right) + \rho_s \eta_{SRE} r_i = 0; \; i = C_2H_5OH, H_2O, CO_2 \text{ and } H_2 \tag{25}$$

The net reaction rates (r_i) from Equation (25) can be determined for each chemical component. These rates are shown in Equation (26) below.

$$r_{C_2H_5OH} = -R_{SRE},\ r_{H_2O} = -3R_{SRE},\ r_{CO_2} = +2R_{SRE},\ and\ r_{H_2} = +6R_{SRE} \tag{26}$$

3.9 Numerical solution of the direct problem

The numerical solution of the mathematical model was carried out for a numeric method which ensures numerical stability (Ben Taher et al., 2021). The proposed model was solved by the Finite Volume (FV) method in together with prescribed initial and boundary conditions to analyze the performance of the LPPB reformer.

4. RESULTS AND DISCUSSIONS

The mathematical modelling developed based on the performance from LPPB reformer using the molten salt's thermal energy. The mathematical model depends on very physical parameters. These physical parameters are shown in Table 1 as follows.

Table 1. Physical parameters used to obtain the simulating results.

Identification of parameters	Symbols	Values
Kinetic constant of the SRE	k_{SRE}, kmol/ $kg_{cat.}$sec.$^{(1)}$	1.23×10^{20}
Adsorption constant of $C_2H_5O_{(1)}$	$K_{C2H5O(1)}$, $kPa^{-1/2\,(1)}$	4.14×10^{-6}
Adsorption constant of $CO_{2(1)}$	$K_{CO2(1)}$, $kPa^{(1)}$	6.81×10^{-5}
Adsorption constant of $CO_{(1)}$	$K_{CO(1)}$, $kPa^{(1)}$	1.58×10^{-3}
Adsorption constant of $CH_{4(1)}$	$K_{CH4(1)}$, $kPa^{(1)}$	$1.25 \times 10^{+9}$
Adsorption constant of $HCOO_{(1)}$	$K_{HCOO(1)}$, $kPa^{3/2(1)}$	6.09×10^{-3}
Adsorption constant of H_2	$K_{H2(1)}$, $kPa^{1/2(1)}$	3.12×10^{-4}
Adsorption constant of $C_2H_4O_{(1)}$	$K_{C2H4O(1)}$, $kPa^{-4\,(1)}$	1.01×10^{-2}
Adsorption constant of $HO_{(1)}$	$K_{HO(1)}$, $kPa^{-1/2\,(1)}$	5.12×10^{-3}
Equilibrium constant	K_r, kPa^3	2.11×10^{-16}
Partial pressure of C_2H_5OH	P_{C2H5OH}, kPa	314.01
Partial pressure of H_2	P_{H2}, kPa	124.04
Partial pressure of H_2O	P_{H2O}, kPa	101.67
Partial pressure of CO_2	P_{CO2}, kPa	125.01
Partial pressure of CO	P_{CO}, kPa	72.89
Partial pressure of CH_4	P_{CH4}, kPa	87.17
Steam density	ρ_v, kg/m^3	0.989
Steam specific heat	$C_{p,\,v}$, kJ/kg K	0.741
Steam thermal conductivity	λ_v, W/m K	0.097
Heat transfer coefficient of the steam phase	h_v, W/m^2 K	2.98×10^{-3}
heat transfer coefficient of wall	h_w, W/m^2 K	473.573
Salt density	ρ_{salt}, kg/m^3	1400
Salt specific heat	$C_{p,\,salt}$, kJ/kg K	2.001
Salt thermal conductivity	λ_{salt}, W/m K	0.202
Gaseous mixture density	$\rho_{g,\,mix.}$, kg/m^3	0.6751
Gaseous mixture specific heat	$C_{p,mix.}$, kJ/kg K	16.109
Void fraction of bed	ε_b, m^3 gas/m^3 reformer	0.41
Effective axial thermal conductivity	$\lambda_{ax.,eff}$, W/m K	121.371
Gas-solid heat transfer coefficient	h_{gs}, W/m^2 K	45.73
Solid density	ρ_s, kg/m^3	7750
Solid specific heat	$C_{p,\,s}$, kJ/kg K	423.12
Axial dispersion coefficient of C_2H_5OH	$D_{ax.,g,C2H5OH}$, m^2/sec.	4.927×10^{-3}
Axial dispersion coefficient of H_2O	$D_{ax.,g,H2O}$, m^2/sec.	2.452×10^{-3}
Axial dispersion coefficient of CO_2	$D_{ax.,g,CO2}$, m^2/sec.	4.091×10^{-3}
Axial dispersion coefficient of H_2	$D_{ax.,g,H2}$, m^2/sec.	1.123×10^{-4}

(1) measured at 425°C

Table 1. Physical parameters used to obtain the simulating results (Continuity).

Identification of parameters	Symbols	Values
Mass transfer coefficient of C_2H_5OH	$k_{gs,C2H5OH}$, m/sec.	2.523×10^{-2}
Mass transfer coefficient of H_2O	$k_{gs,H2O}$, m/sec.	1.917×10^{-2}
Mass transfer coefficient of CO_2	$k_{gs,CO2}$, m/sec.	2.071×10^{-2}
Mass transfer coefficient of H_2	$k_{gs,H2}$, m/sec.	1.011×10^{-2}
Effective mass transfer coefficient of C_2H_5OH	$k_{gs,C2H5OH,\ eff}$, m/sec.	2.989×10^{-2}
Effective mass transfer coefficient of H_2O	$k_{gs,H2O,\ eff}$, m/sec.	2.325×10^{-2}
Effective mass transfer coefficient of CO_2	$k_{gs,CO2,\ eff}$, m/sec.	2.279×10^{-2}
Effective mass transfer coefficient of H_2	$k_{gs,H2,\ eff}$, m/sec.	1.127×10^{-2}
Particle radius	R_p, m	0.0032

(1) measured at 425°C

4.1 Temperature distributions in heating tube

Figure 2 reports the temperature distributions $T_{t,v}$ and T_{salt} along the axial direction at different times during the thermal storage process. The temperature is a physical amount that expresses the thermal energy storage of the atoms or molecules in other material. In this context, there is a thermal energy transfer from vapor phase towards the solid (salt) phase where the molten salt temperature is maintained at a lower level. As results, this can be seen in Figure 2 as follows. Figure 2a reports that temperatures of the vapor and salt phases are kept equals up to around z/L = ± 0.25. After that, temperatures of the vapor and salt phases begin range up to around z/L = ± 0.85. On the other hand, Figure 2b shows that temperatures of the vapor and salt phases are maintained equals until around z/L = ± 0.12. After that, temperatures of the vapor and salt phases begin range up to around z/L = ± 0.75.

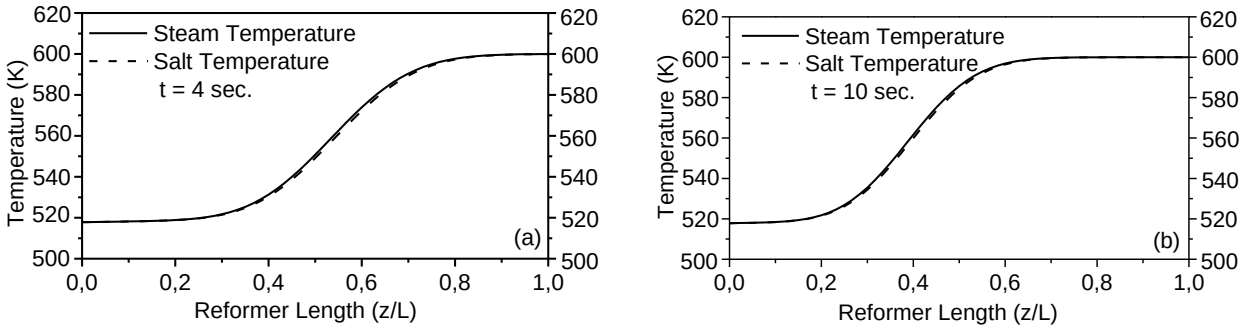

Figure 2. Temperature profiles along the axial direction at different times of the charging process: (a) t = 4 sec, and (b) t = 10 sec.

4.2 Temperature difference and heat flux

Figure 3 presents the change in the temperature difference ($T_{t,\ v}$ - T_{salt}) between fluid and solid and heat flux through the LPPB reformer wall along the axial direction at different charging times.

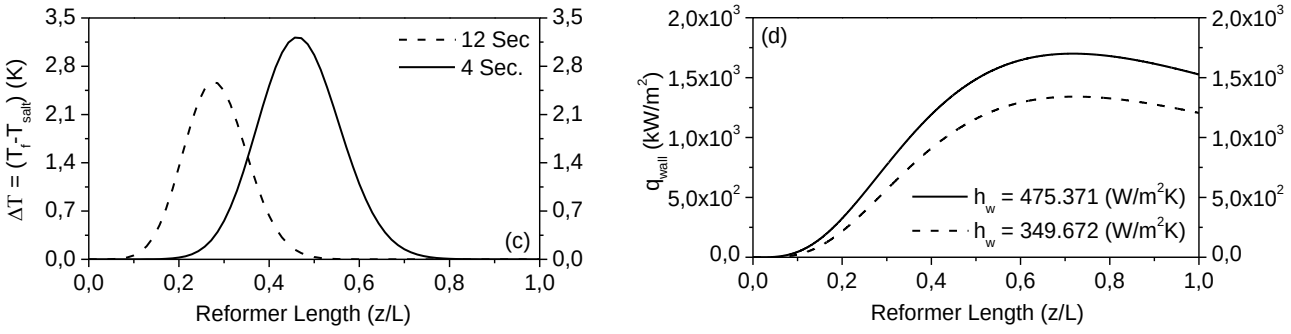

Figure 3. Temperature difference and heat flux: (a) temperature difference along the axial direction at different charging times, (b) heat flux through the LPPB reformer wall.

Figure 3c shows the temperature difference in the LPPB reformer section where the vertical temperature gradient is a local maximum. As results, the temperature difference is reduced when the charging time is increased. On the other hand, Figure 3d demonstrates the heat flux profiles through the LPPB reformer wall at different charging times. The results obtained show that the higher heat transfer coefficient between the vapor and LPPB reformer wall indicates a higher heat flux through the LPPB reformer wall.

4.3 Temperature distributions and concentration distributions in LPPB reformer

Figure 4 shows the temperature profiles of the reaction and solid phase, as well as the concentration profiles of the reactants and products in the LPPB reformer. Figure 4e describes the temperature profiles of the solid phase and chemical reaction along the axial direction from LPPB reformer. As results, the profile of reaction mixture temperature (Trm) reports higher result due to the thermal energy storage of the gaseous mixture. Figure 4f shows the variations the concentration profiles of chemical components in the gaseous mixture along the LPPB reformer. The results indicated a decrease of reactants (C_2H_5OH and H_2O) and an increase from products (CO_2 and H_2).

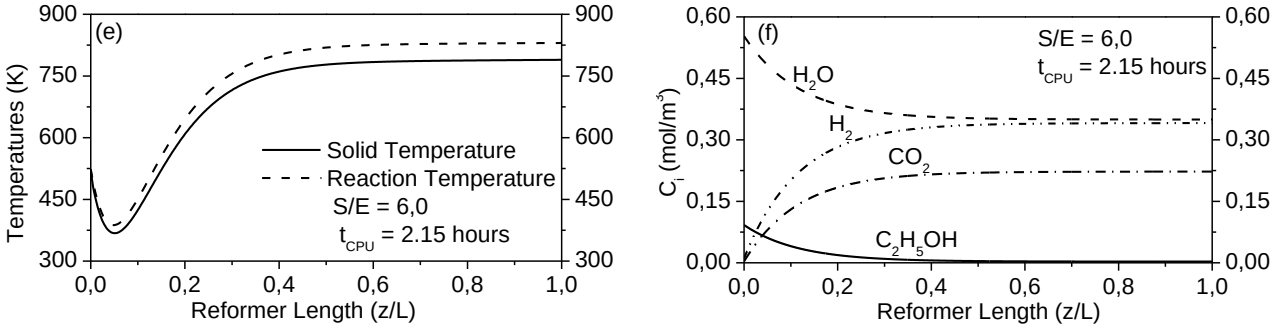

Figure 4. Temperatures of the gas and solid phases and distributions of chemical components: (a) comparison between the temperature profiles of the gas and solid phases inside the LPPB reformer, (b) concentration profiles of the reactants and products at inlet temperature of 873 K.

4.4 Model validation

The model equations are numerically solved by FV method, and the results obtained are validated against experiments from the literature. The simulating results are computed from a computer code developed by authors. The basic data for validation are given by Liu et al., Press (2022). Figure 5g shows a comparison between the numerical results and results from literature for the conversion of C_2H_5OH. On the other hand, Figure 5h has reported a comparison between the numerical results and results from literature for the yield of H_2.

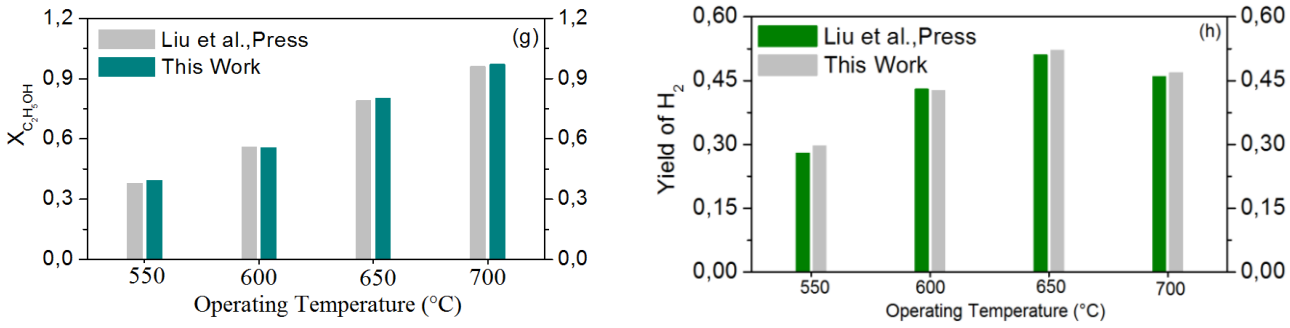

Figure 5. Model validation by comparison between the numerical simulation and experimental data: (a) conversion C_2H_5OH, (b) yield of H_2.

4.5 Uncertainty quantification

After driving a validation by comparative analysis of the conversion of C_2H_5OH and yield of H_2 using data of the literature, the optimal fitting value and confidence interval of the observed data were obtained. The plots of the conversion of C_2H_5OH and yield of H_2 are reported in Figure 6. In this figure, an uncertainty level of 5% is assumed for the robustness analysis. Based on the simple linear regression model, the uncertainty of the conversion of C_2H_5OH and

Yield of H_2 are analyzed, and statistical parameters on the 95% confidence interval are computed how is shown in Table 2. It can be seen in Figure 6i that the conversion of C_2H_5OH has been fitted to the data of the literature for a 5% uncertainty level. The correlation coefficient (R), determination coefficient (R^2), and adjusted determination coefficient $(R^2)_{Adj.}$ are measurements used to explain as the variability of one variable can be impacted by its relationship to another related variable. The Standard Deviation (SD) indicates the degree of the uncertainty when a random variable or a set of data that is measured. A low SD shows that the values tend to be close to the mean of the set, while a high SD indicates that the values are spread out over a wider range. As results of these statistical indicators, Table 2 shows the statistical indicators for the conversion of C_2H_5OH and yield of H_2.

Table 2. Statistical analysis with width of the 95% confidence interval for the conversion of C_2H_5OH and Yield of H_2.

Statistical parameters	Conversion fit of C_2H_5OH	Yield fit of H_2
R	0.9998	0.9969
R^2	0.9995	0.9941
$R^2_{Adj.}$	0.9993	0.9912
SD	0.0067	0.0091

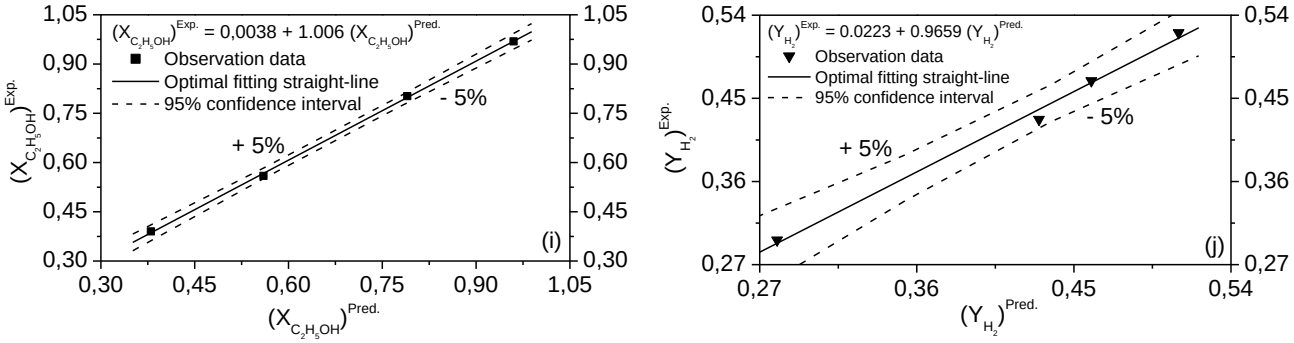

Figure 6. Uncertainty analysis of the conversion of C_2H_5OH and yield of H_2: (i) conversion fit of C_2H_5OH to the data of the literature, (j) yield adjustment of H_2 to the data of the literature.

5. CONCLUSIONS

The work has focused on a 1D transient mathematical model based on heat transfer process to numerically investigate the profiles of temperature of the thermal charge in the heating tube. Besides, a second 1D pseudo-homogeneous mathematical model was developed based on the heat and mass transfer coupled to a kinetic model of the SRE in LPPB reformer. The numerical analysis was made using the FV technique in which the energy balance equations inside the heating tube were coupled with the energy and mass balance equations through the heat flux that passes by the LPPB reformer wall. Therefore, key conclusions of this study include:

1. The thermal energy storage inside the heating tube is transferred towards reaction zone through the heat flux that passes by the LPPB reformer wall. As a result, the heat flux drives the SRE process due to the endothermic reaction.
2. The profile of reaction mixture temperature (Trm) has been indicated higher thermal energy storage in the gaseous mixture where the production of H_2 achieves 34. 29% at inlet temperature of 873 K.
3. The validation of the computer code has been shown that the conversion of C_2H_5OH increases as the operating temperature increases. While, the yield of H_2 has been indicated an oscillation with an increase of the operating temperature. Besides, the uncertainty degree of the conversion of C_2H_5OH is lesser than the uncertainty degree of the yield of H_2.

6. ACKNOWLEDGEMENTS

The authors are grateful to University of Pernambuco for the financial support given (Project 127/2019).

7. REFERENCES

Aron, N. S. M., Khoo, K. S., Chew, K. W., Show, P. L., Chen, W-H., Nguyen, T. H. P., 2020. "Sustainability of the four generations of biofuels - A review". *Inter J Energy Research*, Vol. 44 (12), pp. 9266-9282.

Ben Taher, M. A., El-Otmany, H., El Rhafiki, T., Kousksou, T., Zeraouli, Y., 2021. "Inverse method to describe crystallization of undercooled water in cold storage tank". *J. of Energy Storage*, Vol. 36, p. 102404.

Cruz, B. M. and Silva, J. D., 2017. "A two-dimensional mathematical model for the catalytic steam reforming of methane in both conventional fixed-bed and fixed-bed membrane reformers for the production of hydrogen". *Int J Hydrogen Energy*, Vol. 42, pp. 23670-23690.

Chein, R. Y., Hsu, W. H. and Yu, C. T., 2017. "Parametric study of catalytic dry reforming of methane for syngas production at elevated pressures". *Int J Hydrogen Energy*, Vol. 42, pp. 14485-14500.

Dias, V. F., Silva, J. D., 2020. "Mathematical modelling of the solar ‐ driven steam reforming of methanol for a solar thermochemical micro - fluidized bed reformer: thermal performance and thermochemical conversion". *J Braz Soc Mech Sci Eng*, Vol. 42, p. 447.

He X., Qiu J., Wang W., Hou Y., Ayyub M., Shuai Y., 2022. "A review on numerical simulation, optimization design and applications of packed-bed latent thermal energy storage system with spherical capsules". J Energy Storage, Vol. 51, p. 104555.

Lima, K. P. M., Dias, V. F., Silva. J. D., 2020. "Numerical modelling for the solar driven bi-reforming of methane for the production of syngas in a solar thermochemical micro-packed bed reactor". *Int J Hydrogen Energy*, Vol. 45, pp. 10353-10369.

Liu, H., Li, H., Li, S., Press. "Ni-hydrocalumite derived catalysts for ethanol steam reforming on hydrogen production". Int J Hydrogen Energy, Vol. xx, pp. xxx.

Sahoo D. R., Vajpai S., Patel S., K.K. Pant K. K., 2007. "Kinetic modeling of steam reforming of ethanol for the production of hydrogen over Co/Al2O3 catalyst". *Chem Eng J*, Vol. 125, pp. 139-147.

Silva, J. D. and Abreu, C. A. M., 2016. "Modelling and simulation in conventional fixed-bed and fixed-bed membrane reactors for the steam reforming of methane". *Int J Hydrogen Energy*, Vol. 41, pp. 11660-11674.

Silva, J. D. and Abreu, C. A. M., 2016. "Modelling and simulation in conventional fixed-bed and fixed-bed membrane reactors for the steam reforming of methane". *Int J Hydrogen Energy*, Vol. 41, pp. 11660-11674.

Sun B., Liu Z., Ji X., Gao L., Che D., 2022. "Thermal energy storage characteristics of packed bed encapsulating spherical capsules with composite phase change materials". *Appl Ther Eng*, Vol. 201, p. 117659.

Villafán-Vidales H. I., Arancibia-Bulnes C. A., Riveros-Rosas D., Romero-Paredes H., Estrada C. A., 2017. "An overview of the solar thermochemical processes for hydrogen and syngas production: Reactors and facilities". *Ren Sust Energy Reviews*, Vol. 75, pp. 894-908.

8. RESPONSIBILITY NOTICE

The author(s) is (are) the only responsible for the printed material included in this paper.